Nanomaterials and Nanotechnology

OPEN ACCESS
ARTICLE

Facile Preparation of Silver Halide Nanoparticles as Visible Light Photocatalysts

Regular Paper

Linfan Cui[1], Tifeng Jiao[1,2,3]*, Qingrui Zhang[1]*, Jingxin Zhou[1] and Qiuming Peng[2]

1 Hebei Key Laboratory of Applied Chemistry, School of Environmental and Chemical Engineering, Yanshan University, Qinhuangdao, P. R. China
2 State Key Laboratory of Metastable Materials Science and Technology, Yanshan University, Qinhuangdao, P. R. China
3 National Key Laboratory of Biochemical Engineering, Institute of Process Engineering, Chinese Academy of Sciences, Beijing, P. R. China
*Corresponding author(s) E-mail: tfjiao@ysu.edu.cn; zhangqr@ysu.edu.cn

Received 04 February 2015; Accepted 27 May 2015

DOI: 10.5772/60910

Abstract

In this study, highly efficient silver halide (AgX)-based photocatalysts were successfully fabricated using a facile and template-free direct-precipitation method. AgX nanoparticles, which included silver chloride (AgCl), silver bromide (AgBr) and silver iodide (AgI), were synthesized using different potassium halides and silver acetate as reactive sources. The size distribution of the AgX nanoparticles was determined by the reaction time and ratio of the reagents, which were monitored by UV-vis spectra. The as-prepared AgX nanoparticles exhibited different photocatalytic properties. This shows the differences for the photodegradation of methyl orange and Congo red dyes. In addition, the AgCl nanoparticle-based photocatalyst exhibited the best photocatalytic property among all three types of AgX nanoparticles that are discussed in this study. Therefore, it is a good candidate for removing organic pollutants.

Keywords Nanostructure, Silver halide, Photocatalyst, Nanoparticle

1. Introduction

Photocatalysts have been widely used in water and air purification to remove organic pollutants [1-6]. The organic pollutants include, but are not limited to, organic dyes, organic pesticides and organic herbicides. They do not easily decompose under atmosphere conditions. This has a negative impact on the environment. The photocatalytic approach has been considered as a cost-effective alternative strategy for decomposing organic pollutants that are involved in wastewater.

The efficiency of a photocatalytic reaction is determined by the catalytic activity of the photocatalyst. The photocatalyst can be a semiconductor, which can create electron-hole pairs under photo-illumination [7]. Additionally, in recent years, researchers have investigated the catalysts of oxides. This is because their large band gap can make the catalysts chemically stable and they have a strong resistance to corrosion, which is induced by surrounding environments. For instance, titanium dioxide (TiO_2)-based catalysts have been widely used for the photodegradation of organic pollutants [8-13]. The band gap of TiO_2 is 3.2 eV. This

belongs to the wide band gap semiconductor. The material needs external energy to generate electron-hole pairs. Thus, the TiO_2-based catalysts with large band gaps require a high-energy ultraviolet (UV) light to be activated. When only solar irradiation is readily available, this leads to low-efficiency. In recent years, intensive research efforts have been made to enhance the absorption coefficient of the catalysts that are in both visible and near infrared regions. The catalytic performance requires further improvement for practical applications [14-19]. In contrast, the plasmonic photocatalysts that are made of noble metals nanoparticles exhibit high absorption coefficients in a broad UV–visible–near infrared spectral range. This is due to their strong surface plasmon resonance (SPR) [20-22]. In particular, as a plasmonic photocatalyst, silver nanoparticles show efficient plasmon resonance in the visible region [23, 24].

Silver halides (AgX) are highly photosensitive semiconductors. They have been extensively used as photosensitizers and source materials in photographic films. They can also be used as metallic silver precursors [25]. When photons are absorbed, AgX produces an electron and a hole. This causes an electron transfer and, subsequently, the Ag^+ may transform into Ag^0. For example, Ag/AgX are photocatalysts that can be obtained from AgX by exploiting their photosensitivity. The photocatalysts are highly efficient and stable under visible-light illumination [26, 27]. Despite the fact that their band gaps are higher than the edge of visible light, AgX is also supposed to be a visible light photocatalytic material [28]. This is due to their good photosensitivity. In this study, AgX nanoparticles, including silver chloride (AgCl), silver bromide (AgBr) and silver iodide (AgI), were fabricated using a facile and template-free direct-precipitation method in dark atmosphere conditions. The photocatalytic properties of the as-prepared AgX nanoparticles were also investigated and compared. These AgX nanoparticles-based photocatalysts were found to promote the degradation of methyl orange (MO) and Congo red (CR).

2. Experiment

2.1 Materials

Silver acetate (CH_3COOAg, >99.95 %, Aladdin, A. R., Shanghai), potassium chloride, potassium bromide, potassium iodide (KCl, KBr, KI, >99.5 %, Beijing Chemical Works, A. R.), methyl orange (MO, 96%, Aladdin, Shanghai) and Congo red (CR, >98 %, Aladdin, Shanghai) were used as they were received, without additional purification. In all cases, deionized water (18.2 MΩ cm) from Milli-Q Academic water purification system (Millipore Corp., Billerica, MA, USA) was used.

2.2 AgX Preparation

To synthesize the AgCl nanoparticles, a 500 μL aqueous solution of KCl (0.2 M) was injected dropwise into a 10 mL aqueous solution of CH_3COOAg (0.01 M) at room temperature, using vigorous magnetic stirring within ~five minutes. The solution mixture was stirred continuously for another 0.5, three and six hours, respectively. The reaction vessel was placed in a dark area to prevent the formation of metallic Ag^0. The initial KCl to CH_3COOAg ratios were fixed at 2:1 and 1:2. Subsequently, the reactants were collected using centrifugation and washed by ultrapure water. The solid products were dried at 65 ^oC for 12 hours. Synthesis of AgBr and AgI was achieved using KBr and KI reagents, respectively, via the same procedure as described above.

2.3 Characterization

The sample morphology was characterized using a field emission scanning electronic microscope (FESEM, Hitachi S-4800, Japan) with an accelerating voltage of 5–15 kV and a transmission electron microscopy (TEM, JEOL TEM-2010, Japan) with an accelerating voltage of 200 kV. The energy dispersive X−ray spectroscopy (EDX) was measured with a Horiba EMAX X−act energy dispersive spectroscopy that was attached to the Hitachi S−4800 system. The growth of the AgX nanostructures was monitored using ultraviolet absorption spectra (Shimadzu UV-2550, Japan). The X-ray diffraction (XRD) pattern (Rigaku D/max 2550PC Rigaku, Tokyo, Japan) was obtained using a Cu Kα radiation with an incident wavelength of 0.1542 nm under a voltage of 40 kV and a current of 200 mA. The scan rate was 0.5 degree per minute.

2.4 Photocatalytic Activity

Approximately 20 mg as-prepared AgX nanoparticles were added into 100 mL, 10 mg/L, MO or CR aqueous solution. A 250 W high pressure mercury lamp was employed as the light source. The power density was 80 W/cm and the effective range of the emission wavelength was 350-370 nm. The degradation process of MO or CR in the aqueous solution with the presence of photocatalysts was determined by monitoring the absorption peaks at 465 nm and 497 nm wavelengths, for MO and CR, respectively.

3. Results and Discussion

Fig. 1 shows the cube-like nanostructured AgCl with different sizes and morphology, using a KCl to CH_3COOAg ratio of 1:1. Fig. 1a shows the aggregates of the small particles when the reactants were collected after about 0.5 hours. The particles were close to the cube-like structure and their sizes were not uniform. Different mixing times were fixed to investigate the influence on the morphology of AgCl. The cube-like AgCl nanoparticles, with an average diameter of ca. 150 nm, were observed when the reactant solution was stirred for three hours (Fig. 1b). A prolonged mixing time (i.e., six hours) resulted in a non-uniform structure and serious agglomeration, as shown in Fig. 1c. The size of the nanoparticle was larger than that of three hours. It seems that the AgCl nanoparticle became larger

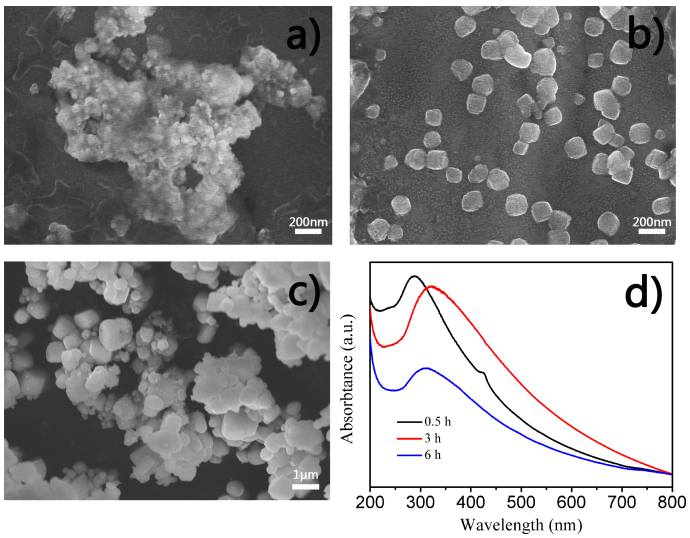

Figure 1. SEM images and UV–vis spectra of AgCl nanoparticles, collected after mixing KCl and CH_3COOAg aqueous solution with a ratio of 1:1 for different periods of time. (a) 0.5, (b) three, (c) six hours, (d) UV–vis spectra.

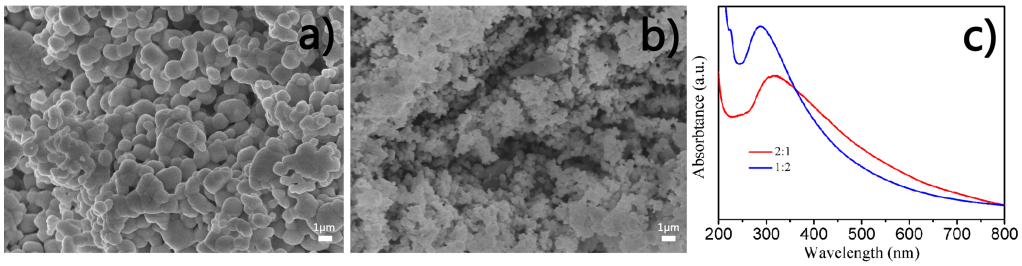

Figure 2. SEM images and UV–vis spectra of AgCl nanoparticles with different KCl to CH_3COOAg ratios. (a) 2:1, (b) 1:2 after mixing of three hours, (c) UV–vis spectra.

when the mixing time was prolonged. Thus, a suitable reaction time will positively affect the preparation of AgCl. The reactions of different reactant ratios were also evaluated. Fig. 2a and 2b show the morphology of the AgCl samples, which were produced using KCl to CH_3COOAg ratios of 2:1 and 1:2, respectively. These AgCl nanoparticles aggregated into large clusters, which prevented an accurate estimation of their morphology and size distributions. This suggests that the preferred KCl to CH_3COOAg ratio is 1:1. The UV-vis spectra of the samples are shown in Fig. 1d and Fig. 2c. The broad and strong absorption at 200–350 nm could be ascribed to the characteristic absorption of the AgCl semiconductors [29]. The shift in the band may have contributed to the different sizes of the AgCl nanoparticles. It is worth noting the absence of absorption at 550 nm in the visible-light region. This suggests that silver nanoparticles were not formed during our experiments.

AgBr and AgI were also synthesized using the same method that was described for the synthesis of AgCl nanostructures. Fig. 3 shows the TEM images and particle size distributions of three different AgX nanoparticles. All of the nanostructures were well distributed. To be specific, a few AgCl nanoparticles with a main size distribution of 130-170 nm were found (Fig. 3d). In contrast, uniform AgBr nanoparticles with a size distribution of 140-180 nm were observed, as shown in Fig. 3e. In addition, for the AgI nanostructures that were generated by KI and CH_3COOH with a ratio of 1:1, the main size distributions were 50-60 nm, as depicted in Fig. 3f. The standard deviations of the AgCl, AgBr and AgI were 48.34, 36.74 and 11.17.

To validate the generation of AgX nanospecies, the components of the nanostructures were investigated by EDX. The x- and y- axis labels were energy/keV and counts/cps, respectively. As shown in Fig. 4a, the Ag and Cl elements were evidently detected. A semiquantitative analysis showed that the atomic ratio between the Ag and Cl elements was approximately 1:1. The data were in agreement with the theoretic stoichiometric atomic ratio between Ag and Cl species in AgCl. The EDX analyses of AgBr and AgI are shown in Fig. 4b and 4c. The atomic ratio between the Ag and Br elements was 1.01:1. The same result was also achieved for the AgI nanostructures. The XRD patterns of the AgX nanostructures are shown in Fig. 4d. The distinct diffraction peaks at a 2θ of 27.78°, 32.2°, 46.2°, 54.78°, 57.44°, 67.42°, 74.4° and 76.7° could be assigned to the (111), (200), (220), (311), (222), (400), (331) and (420) planes, respectively, for the typical cubic phase of AgCl crystal (JCPDS file 31-1238). This suggests the existence of AgCl species in the synthesized nanostructures. These diffraction peaks were

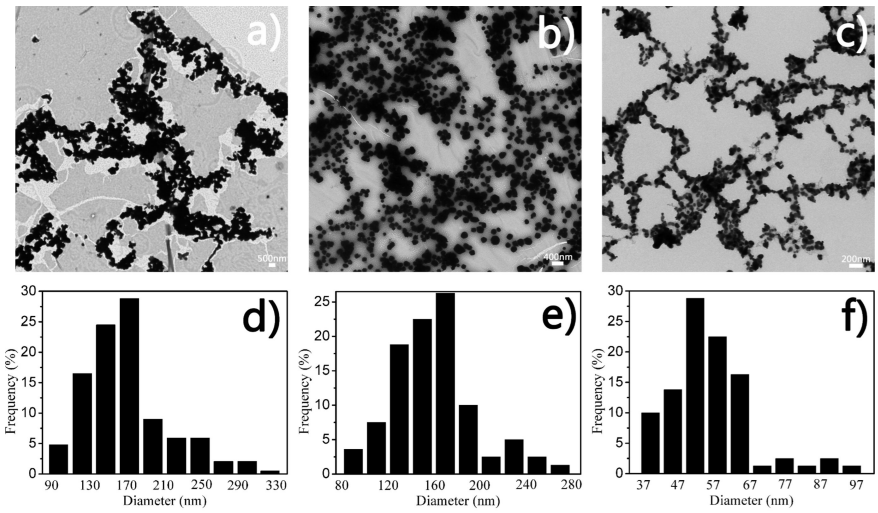

Figure 3. TEM images and particle size distribution histograms of the AgX nanostructures, formed using a 1:1 ratio of reaction mixtures for three hours (a, d) AgCl, (b, e) AgBr, and (c, f) AgI

sharp and intense, indicating a high degree of crystallinity of the AgCl species. Furthermore, an AgBr phase was also unambiguously detected with characteristic 2θ at 26.66°, 31.14°, 44.26°, 54.98°, 64.44° and 73.2°, which correlated to (111), (200), (220), (222), (400) and (420) reflections of the cubic AgBr (JCPDS file 06-0438), respectively. The XRD patterns of the AgI nanostructures also matched the reported data (JCPDS file 09-0374) of β-AgI. It is worth noting that the signal corresponding to metallic Ag^0 was not detected in these XRD patterns. This implies that less or no Ag nanoparticles were formed during the reaction process. The above experimental results clearly indicate the formation of the AgX nanostructures.

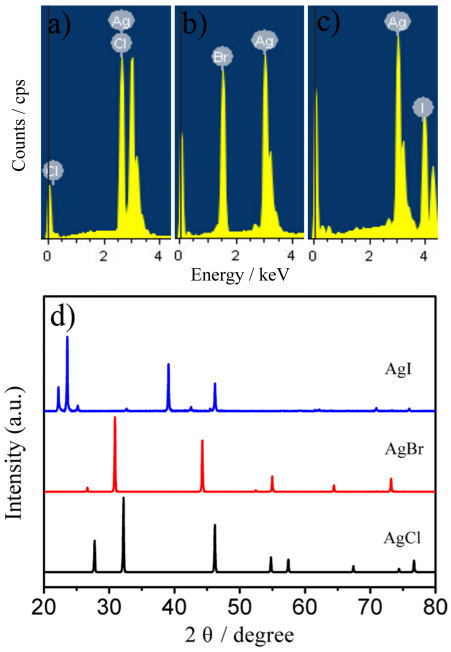

Figure 4. EDX results and XRD spectra for the three species. (a) AgCl, (b) AgBr and (c) AgI nanostructures, (d) XRD spectra.

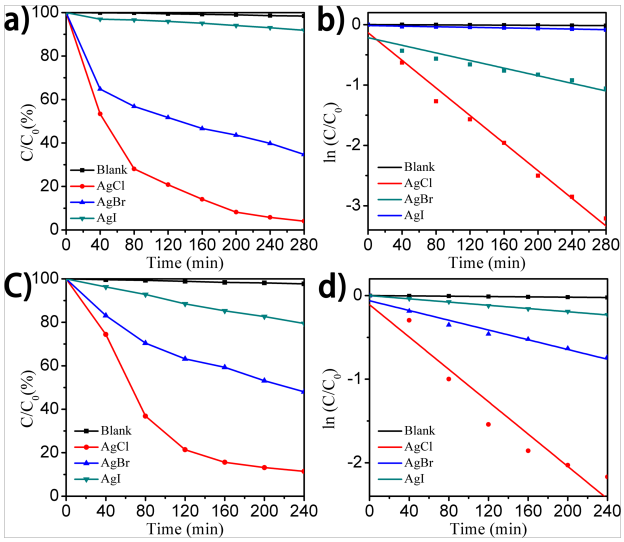

Figure 5. (a, c) Photocatalytic activities and (b, d) kinetic linear simulation curves of AgCl, AgBr, AgI nanospecies for the photodegradation under visible-light irradiation. (a, b) MO, (c, d) CR molecules.

The photocatalytic performances of as-prepared AgX nanostructures for the photodegradation of MO and CR under visible-light irradiation were further investigated. Blank tests were also made under visible-light irradiation and negligible degradation of MO and CR molecules was detected. Fig. 5a and 5c show the plots of concentration (C) of different dyes [i.e., (a) Mo and (c) CR] against the initial concentration (C_0) at the beginning of the reaction versus time. When the AgCl nanospecies were employed as photocatalysts, about ca. 95.97 % of the MO molecules were decomposed after being irradiated for 280 minutes under the current experimental conditions, as shown in Fig. 5a. In contrast, when the AgBr and AgI nanocomposites were used as photocatalysts under the same experimental conditions, ca. 65.29 and 8.15 % MO molecules were decomposed for 280 minutes, respectively. This suggests a significantly higher photocatalytic activity of the AgCl

nanostructures than that of the AgBr and AgI nanospecies. The AgI nanoparticles exhibited fairly weak photocatalytic activity for the degradation of the MO molecules. Furthermore, when AgCl was used as a photocatalyst for the degradation of the CR molecules, about 88.58 % of the CR molecules were decomposed after 240 minutes. This degradation rate was much higher than that of 51.98 % and 20.53 %, when using AgBr and AgI (Fig. 5c), respectively. The plots of $\ln(C/C_0)$ versus the reaction time (t), shown in Fig. 5b and 5d, exhibited a linear relationship. This indicates that the decomposition reaction of the MO and CR molecules follows the first-order kinetics [30]:

$$-\frac{dC}{dt} = kC$$

where C is the real-time concentration, t stands for the reaction time and k represents the rate constant. According to Fig. 5b, the rate constants of the photocatalytic degradation of the MO molecules using AgCl, AgBr and AgI were determined to be 0.0114 $minutes^{-1}$, 0.0032 $minutes^{-1}$ and 0.0002 $minutes^{-1}$, respectively. On the other hand, the rate constants of the photocatalytic degradation of the CR molecules using AgCl, AgBr and AgI were determined to be 0.0101 $minutes^{-1}$, 0.0030 $minutes^{-1}$ and 0.0010 $minutes^{-1}$ (Fig. 5d), respectively. The band gaps of the three AgX nanostructures are different, which may influence the activated process. Thus, their photocatalytic activities may exhibit differences. Furthermore, their photocatalytic processes are related to the energy levels of the conduction band and valance band, the oxidation-reduction potential of adsorbate (Mo and CR molecules) and so on. The morphology and environment of the AgX nanoparticles also have an effect on their photocatalytic properties. Different morphologies lead to different surface areas, which directly determine the photocatalytic activity. Furthermore, different structures may have different catalytically sites [29, 31-33]. During the degradation process, the molecules of the pollutants can influence the surface and structure of the photocatalysts, which then has an effect on their photocatalysis efficiency. In this work, three kinds of AgX nanoparticles were synthesized with different shapes and their morphology could not be directly compared. When these two pollutants were photodegraded, the AgCl nanoparticles had higher photocatalysis efficiency. Additionally, during the process of visible light irradiation, as the colour of the AgCl changed from white to purple, the Ag nanoparticles may have formed on the surface of the AgCl. Under light, the strong photosensitivity of AgX makes it easier for the reduction of Ag^+ to Ag^0. Metal nanostructures with strong SPRs can increase their absorption efficiently in the visible region. The results showed that the AgCl nanoparticles could be used as useful photocatalysts for the degradation of different organic dyes.

4. Conclusion

In summary, this study reported a facile, one-pot direct-precipitation route to fabricate AgX photocatalysts under ambient conditions. The variations of the reaction time and reactant ratio had an important effect on the morphology of the AgX nanostructures. The as-synthesized three nanoparticles displayed different photocatalytic efficiency for catalysing the decomposition of MO and CR under the illumination of the visible light. Among the three AgX species that are discussed in this study, the AgCl exhibited the best catalytic performance. Thus, the as-prepared AgCl could be used as a high-performance visible-light-energized plasmonic photocatalyst for the photodegradation of organic dyes.

5. Acknowledgements

This work was financially supported by the National Natural Science Foundation of China (Nos. 21473153 and 21207112), the Natural Science Foundation of Hebei Province (No. B2013203108), Science Foundation for the Excellent Youth Scholars from Universities and Colleges of Hebei Province (Nos. Y2011113 and YQ2013026), Support Program for the Top Young Talents of Hebei Province and Open Foundation of National Key Laboratory of Biochemical Engineering (Institute of Process Engineering of Chinese Academy of Sciences).

6. References

[1] Fujishima A, Rao T N, Tryk D A (2000) Titanium Dioxide Photocatalysis. J. Photoch. Photobio. C 1: 1-21.

[2] Stafford U, Gray K A, Kamat P V (1996) Photocatalytic Degradation of Organic Contaminants: Halophenols and Related Model Compounds. Heterogen. Chem. Rev. 3: 77-104.

[3] Agustina T E, Ang H M, Vareek V K (2005) A Review of Synergistic Effect of Photocatalysis and Ozonation on Wastewater Treatment. J. Photoch. Photobio. C 6: 264-273.

[4] Gaya U I, Abdullah A H (2008) Heterogeneous Photocatalytic Degradation of Organic Contaminants over Titanium Dioxide: A Review of Fundamentals, Progress and Problems. J. Photoch. Photobio. C 9: 1-12.

[5] Zhang H J, Chen G H, Bahnemann D (2000) Photoelectrocatalytic Materials for Environmental Applications. J. Mater. Chem. 19: 5089-5121.

[6] Ahmed S, Rasul M G, Martens W N, Brown R, Hashib M A (2010) Heterogeneous Photocatalytic Degradation of Phenols in Wastewater: A Review on Current Status and Developments. Desalination 261: 3-18.

[7] Li X, Chen G, Yang L, Zhen Z, Liu J (2010) Multifunctional Au-coated TiO2 Nanotube Arrays as Recyclable SERS Substrates for Multifold Organic

Pollutants Detection Advanced Functional Materials. Adv. Funct. Mater. 20: 2815-2824.

[8] Fujishima A, Honda K (1972) Electrochemical Photolysis of Water at a Semiconductor Electrode. Nature 238: 37-38.

[9] Bhatkhande D S, Pangarkar V G, Beenackers A A C M (2002) Photocatalytic Degradation for Environmental Applications. J. Chem. Technol. Biot. 77: 102−116.

[10] Chen C, Ma W, Zhao J (2010) Semiconductor-mediated Photodegradation of Pollutants Under Visible-light Irradiation. Chem. Soc. Rev. 39: 4206−4219.

[11] Zhang D, Li G, Yu J (2010) Inorganic Materials for Photocatalytic Water Disinfection. J. Mater. Chem. 20: 4529−4536.

[12] Chen X, Mao S (2007) Titanium Dioxide Nanomaterials: Synthesis, Properties, Modifications, and Applications. Chem. Rev. 107: 2891-2959.

[13] Yu H, Irie H, Hashimoto K (2010) Conduction Band Energy Level Control of Titanium Dioxide: Toward an Efficient Visible-light-sensitive Photocatalyst. J. Am. Chem. Soc. 132: 6898–6899.

[14] Zhao W, Ma W, Chen C, Zhao J, Shuai Z (2004) Efficient Degradation of Toxic Organic Pollutants with Ni2O3/TiO2-xBx Under Visible Irradiation. J. Am. Chem. Soc. 126: 4782-4783.

[15] Li D, Haneda H, Hishita S, Ohashi N (2005) Visible-light-driven N−F−codoped TiO2 photocatalysts. 2. Optical Characterization, Photocatalysis, and Potential Application to Air Purification. Chem. Mater. 17: 2596-2602.

[16] Liu G, Chen Z, Dong C, Zhao Y, Li F, Lu G, Cheng H (2006) Visible Light Photocatalyst: Iodine-doped Mesoporous Titania with a Bicrystalline Framework. J. Phys. Chem. B 110: 20823-20828.

[17] Hamal D B, Haggstrom J A, Marchin G L, Ikenberry M A, Hohn K, Klabunde K J (2010) A Multifunctional Biocide/Sporocide and Photocatalyst Based on Titanium Dioxide (TiO2) Codoped with Silver, Carbon, and Sulfur. Langmuir 26: 2805–2810.

[18] Vu T, Mighri F, Ajji A, Do T (2014) Synthesis of Titanium Dioxide/Cadmium Sulfide Nanosphere Particles for Photocatalyst Applications. Ind. Eng. Chem. Res. 50: 3888-3897.

[19] Asahi R, Morikawa T, Irie H, Ohwaki T (2014) Nitrogen-doped Titanium Dioxide as Visible-light-sensitive Photocatalyst: Designs, Developments, and Prospects. Chem. Rev. 114: 9824–9852

[20] Kreibig U, Vollmer M (1995) Optical Properties of Metal Clusters. Springer, Berlin.

[21] Huang X, El-Sayed I H, Qian W, El-Sayed M A (2006) Cancer Cell Imaging and Photothermal Therapy in the Near-infrared Region by Using Gold Nanorods. J. Am. Chem. Soc. 128: 2115-2120.

[22] Zhang Q, Ge J, Pham T, Goebl J, Hu Y, Lu Z, Yin Y (2009) Reconstruction of Silver Nanoplates by UV Irradiation: Tailored Optical Properties and Enhanced Stability. Angew. Chem. Int. Edit. 48: 3516-3519.

[23] Awazu K, Fujimaki M, Rockstuhl C, Tominaga J, Murakami H, Ohki Y, Yoshida N, Watanabe T (2008) A Plasmonic Photocatalyst Consisting of Silver Nanoparticles Embedded in Titanium Dioxide. J. Am. Chem. Soc. 130: 1676-1680.

[24] Georgekutty R, Seery M K, Pillai S C (2008) A Highly Efficient Ag-Zno Photocatalyst: Synthesis, Properties, and Mechanism. J. Phys. Chem. C 112: 13563-13570.

[25] Grzelczak M, Liz-Marzan L M (2014) The Relevance of Light in the Formation of Colloidal Metal Nanoparticles. Chem. Soc. Rev. 43: 2089-2097.

[26] Wang P, Huang B, Qin X, Zhang X, Dai Y, Wei J, Whangbo M (2008) Ag@Agcl: A Highly Efficient and Stable Photocatalyst Active Under Visible Light. Angew. Chem. Int. Edit. 47: 7931–7933.

[27] An C, Peng S, Sun Y (2010) Facile Synthesis of Sunlight-driven AgCl:Ag Plasmonic Nanophotocatalyst. Adv. Mater. 22: 2570-2574.

[28] Lan Y H, Qian X Z, Zhao C J, Zhang Z M, Chen X, Li Z (2013) High Performance Visible Light Driven Photocatalysts Silver Halides and Graphitic Carbon Nitride (X = Cl, Br, I) Nanocomposites. J. Colloid. Interf. Sci. 395:75-80.

[29] Wang P, Huang B, Lou Z, Zhang X, Qin X, Dai Y, Zheng Z, Wang X (2010) Synthesis of Highly Efficient Ag@AgCl Plasmonic Photocatalysts with Various Structures. Chem. Eur. J. 16: 538-544.

[30] Zhu M, Chen P, Liu M (2012) Highly Efficient Visible-light-driven Plasmonic Photocatalysts Based on Grapheneoxide-hybridized One-dimensional Ag/AgCl Heteroarchitectures. J. Mater. Chem. 22: 21487− 21494.

[31] Zhu M, Chen P, Ma W, Lei B, Liu M (2012) Template-free Synthesis of Cube-like Ag/AgCl Nanostructures via a Direct-precipitation Protocol: Highly Efficient Sunlight-driven Plasmonic Photocatalysts. ACS Appl. Mater. Interfaces 4: 6386-6392.

[32] Li Y, Liu Q, Shen W (2011) Morphology-dependent Nanocatalysis: Metal Particles. Dalton Trans. 40: 5811−5826.

[33] Liu Y, Fang L, Lu H, Li Y, Hu, C, Yu H (2012) One-pot Pyridine-assisted Synthesis of Visible-light-driven Photocatalyst Ag/Ag3PO4. Appl. Catal. B: Environ. 115−116: 245−252.